Macromolecules

Article

pubs.acs.org/Macromolecules

Poly(ether−thioethers) by Thiol−Ene Click and Their Oxidized Analogues as Lithium Polymer Electrolytes

Joel M. Sarapas and Gregory N. Tew*

Department of Polymer Science and Engineering, University of Massachusetts, Amherst, Massachusetts 01003, United States

Supporting Information

ABSTRACT: A family of nine poly(ether−thioethers) (PETEs) were synthesized by the radical coupling of a dithiol and a divinyl ether to investigate the importance of organosulfur incorporation in solid polymer electrolytes. Two series of four polymers each were synthesized to probe both the effect of the carbon spacer length between thioether units and of the ratio of ether to thioether units. PETE samples from these two series had low T_g values, ranging from −50 to −75 °C, and all but two PETEs displayed crystallinity. Molecular weights between 7 and 13 kg/mol were obtained for all polymers. Taking advantage of the sulfur-centered functional group, a single polymer, **PETE-1**, was selectively oxidized to the poly(ether−sulfoxide) **PESO-1** and the poly(ether−sulfone) **PES-1**. Oxidation increased the T_g of **PETE-1** from −64 °C to −36 and −26 °C for **PESO**-1 and **PES**-1, respectively, while all three were amorphous. Of the nine new PETE polymers, two were amorphous and the addition of LiTFSI decreased the extent of crystallinity for the other seven PETE samples. An increase in T_g was also observed for **PETE-1**, **PESO-1**, and **PES-1** with the addition of salt. PETE samples with carbon spacers of two, four, and six methylene units had generally uniform ion conductivity, near 5×10^{-5} S/cm at 80 °C, while the sample with eight methylene units had a lower conductivity that was further decreased by crystallinity at lower temperatures. Samples with varied ether and thioether ratios also had very uniform conductivities, similar in magnitude to samples with varied carbon spacers. Within the oxidized series, **PETE-1** outperformed **PES-1**, which in turn outperformed **PESO-1** in terms of ion mobility. The highest observed conductivity (10^{-4} S/cm) at 80 °C was for **PETE-1** with a salt loading of r = 0.05. The synthetic approach described here will enable a wealth of new polymer structures to be produced with controlled functional group placement and density providing novel materials for solid polymer electrolytes, broad functional group variation, and comprehensive structure−activity relationships.

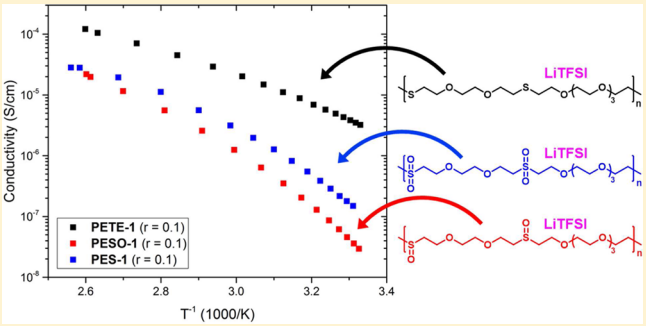

INTRODUCTION

Solid polymer electrolytes (SPEs) are materials capable of dissolving and facilitating the movement of ions.[1,2] SPEs have been especially well studied as separators for lithium ion batteries due to their low toxicity, low flammability, and lack of volatile solvents. Poly(ethylene oxide) (PEO) in particular is known among SPEs to conduct lithium ions well and has been extensively studied as a linear homopolymer as well as in a wealth of architectures including block copolymers, dendrimers, graft copolymers, multiblock copolymers, and star polymers.[3−9] Several systems utilizing short oligo-ethylene oxide side chains from methacrylate, PDMS, phosphazine, and norbornene based monomers have also been developed.[9−12] However, PEO based materials fall short compared to their liquid electrolyte counterparts, with ion conductivities several orders of magnitude too low for many commercial applications.

Efforts to develop new, better conducting SPEs, not reliant on alkylene oxide backbones, are usually hampered by high glass transition temperatures that come with the polar functional groups required to coordinate lithium ions.[2] Regardless, several elegant platforms have been developed that rival PEO conductivity, mostly focusing on polycarbonate and polyester backbones.[13−18] DeSimone and co-workers also developed and tested a series of carbonate end-capped perfluoropolyethers.[19] These polymers displayed extremely low T_g values (∼−100 °C), as well as transference numbers approaching 1, due to the strong polymer−TFSI anion interaction. Surprisingly, polymeric thioethers (alkylene sulfides) have received almost no attention for ion transport systems. In 1986, Clancy et al. described the synthesis of a series of polyalkylene sulfides through a dibromo-/dimercaptoalkane condensation reaction and subsequent Ag^+ conductivity.[20] Similar conductivities were found when compared to other Ag^+−PEO systems. With respect to Li^+, Johansson showed that from a computational standpoint polythioethers may in fact demonstrate improved conductivity over PEO due to the large atomic size of sulfur and lower binding strength to lithium ions.[21] However, it was cautioned that due to the lower

Received: November 20, 2015
Revised: January 27, 2016
Published: February 4, 2016

DOI: 10.1021/acs.macromol.5b02513
Macromolecules 2016, 49, 1154−1162

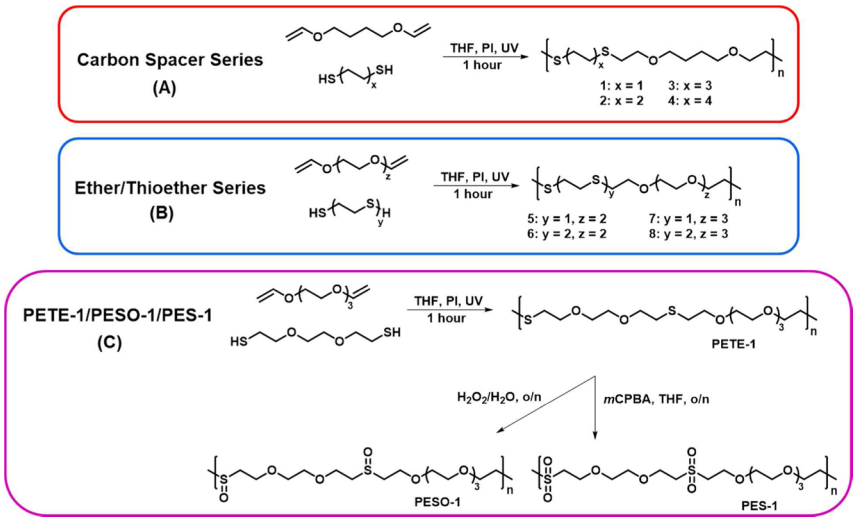

Figure 1. Synthetic approach of polymers **1**−**8** as well as **PETE-1** and its oxidized products, **PESO-1** and **PES-1**. Polymers are grouped by their isolated variable: (A) for the carbon spacer between thioether units, (B) for the ratio of ethers to thioethers, and (C) for the polarity of sulfur centered group. *n* indicates the degree of polymerization and varies between samples.

binding strength, lithium ion solubility in polythioethers may be limited. Therefore, generating polymers with the appropriate balance to solubilize lithium salts yet provide enough ion mobility from thioether functional groups is expected to be nontrivial. In this context, it should be noted that small molecule sulfones and sulfoxides have attracted attention as potential alternatives to traditional carbonate solvents for lithium ion batteries due to their high conductivities and electrochemical stability.[22,23] The high polarity of these functional groups tends to lead to higher T_g materials, which has likely limited the number of reports in the literature discussing sulfoxide and sulfone containing SPEs. In one rare example, Allcock and co-workers reported high-T_g polyphosphazines containing sulfoxides and sulfones that were relatively poor lithium ion conductors without the addition of a plasticizer.[24] Here, we present the design, synthesis, physical properties, and lithium ion conductivities for a series of mixed heteroatom poly(ether−thioethers) (PETE). We also investigate low-T_g sulfone and sulfoxide containing polymers derived from a single PETE and the electrolyte behavior of the resulting polymers.

To achieve the polymers in this work, a step-growth thiol−ene polymerization was employed. The addition of a thiol across a double bond is a powerful and well-studied chemical tool, ranging broadly in application.[25−27] This reaction, when promoted by a radical, proceeds rapidly and largely in the absence of side products, as shown in 2007 by Schlaad and coworkers.[28] Though the reaction itself has been known for over 100 years, its use and popularity in polymer synthesis have recently increased. Most commonly, the radical thiol−ene reaction has been used for the formation of networks due to the variety of available multifunctional thiol and ene reagents, the mild conditions under which the reaction proceeds, and the ability for thiols to participate in orthogonal, nucleophilic additions.[25,29−31] Additionally, postpolymerization functionalization using radical thiol−ene click chemistry has given rise to a plethora of highly varied and modular polymer structures with a range of functional groups.[25,27] More recently, thiol−ene and thiol−yne polymerizations have been extended to polymer−polymer conjugation.[29,32,33] However, substantially less effort has focused on the formation of linear, step-growth polymers by the radical thiol−ene addition.

Marvel and co-workers were the first to identify the addition of a thiol across a double bond as a potential reaction to produce linear polythioethers.[34−41] Recently, Deubel et al. reported the step-growth polymerization of a series of polythioethers from α,ω-alkylene thiols.[42] This synthesis produced polymers with well-defined structure and allowed for control of the carbon spacer between thioether units. In this work, we employed a two monomer step-growth polymerization strategy, using a variety of dithiols and divinyl ethers resulting in two different series of PETEs (see Figure 1): (A) one in which the carbon spacer length between thioethers is varied, while maintaining a constant spacer length between ethers, and (B) the other with constant spacer lengths between heteroatoms but with a varied ratio of ethers to thioethers. The carbon spacer length for alkylene oxide polymers is known to have an important effect on ion conductivity, and the first series was designed to test the impact of spacer length on thermal properties and electrolyte behavior.[43] Likewise, polymers made with varying ratios of thioethers and ethers were examined to determine the effect the two heteroatoms and their ratio had on crystallization and conductivity. Another three samples, representing the third series (Figure 1C), **PETE-1**, **PESO-1**, and **PES-1**, were prepared and characterized to determine the effect of the polarity of the sulfur centered groups on ion mobility. All three polymer series were assessed for conductivity at three different salt loadings.

EXPERIMENTAL SECTION

General. A Blak-Ray 100 W B-110 AP/R lamp was used to irradiate samples for photopolymerization. ^{1}H NMR was acquired using a Bruker 500 MHz Ascend retrofitted with a cryo-probe. FTIR was performed using a PerkinElmer Spectrum 100 FTIR spectrometer with a Universal ATR sampling accessory. GPC of the **1**−**8** was performed using an Agilent 1260 series system equipped with both a refractive index (RI) and an ultraviolet (UV) detector, a PL Gel 5 μm guard column, two 5 μm analytical Mixed-C columns, and a 5 μm analytical Mixed-D column (Agilent). All columns were connected in series and incubated at 40 °C. THF was used as the eluent with a flow rate of 1.0 mL/min. GPC data of **PETE-1**, **PESO-1**, and **PES-1** were obtained using an Agilent Technologies 1260 Infinity, fitted with a PL

DOI: 10.1021/acs.macromol.5b02513
Macromolecules 2016, 49, 1154−1162

Gel 5 μm guard column, a PL Gel 5 μm mix D 1° column, and a PL Gel 5 μm Mix C 1° column. Columns were maintained at 50 °C in a mobile phase of DMF with 0.1 M LiCl. All molecular weights were determined using PS standards. TGA of all samples was acquired using a Thermal Instruments Q50, with a N_2 sample flow rate of 60 mL/min and balance flow rate of 40 mL/min. DSC of all samples was acquired using a Thermal Instruments Q200 DSC with a liquid nitrogen cooling system and a N_2 sample flow rate of 50 mL/min. For each sample, 1−3 mgs were loading into aluminum pans, hermetically sealed, and run using a heat/cool/heat method. Samples were heated to 120 °C at a heating rate of 10 °C/min, cooled to −100 °C at a rate of 5 °C/min, and finally heated again to 120 °C at a rate of 10 °C/min. The final heating curve was used for thermal property evaluation. For EIS measurements, aluminum mounts were initially sputter coated with gold using a Cressington 108 sputter coater. Samples were placed between two mounts inside a spacer cut from PTFE tape with a small hole in the center. The sample was then loaded into a custom system that multiplexes the impedance analyzer to one of eight temperature-calibrated positions within a Cascade TEK TVO-2 vacuum oven. Samples were heated under vacuum and held at 120 °C for 4 h in order to remove any residual solvent or moisture and then allowed to cool to ambient temperature. Impedance spectra in the frequency range of 10 MHz−0.1 Hz were recorded for each sample at repeated time intervals of 30 min during the experiment. The bulk resistance to ion conduction, R, was extracted by fitting a constant function to the first plateau of the impedance magnitude occurring at high frequencies; conductivity was then computed from the known sample area, A = 0.072 cm^2, and thickness of the spacer tape, d = 0.029 cm, as $\sigma = d/(AR)$. All chemicals were purchased from Sigma-Aldrich, Alfa Aesar, Acros Organics, TCI, and BASF and were used without further purification. Electrochemical stability studies were performed using a single-compartment three-electrode cell with a platinum flag as the counter electrode, a nonaqueous Ag/Ag+ reference electrode (calibrated versus ferrocene/ferrocenium (Fc/Fc^+) standard redox couple as an external standard), and a platinum button (0.02 cm^2) as the working electrode. Cyclic voltammetry measurements were carried out on a BASi Epsilon potentiostat scanning voltage from −1.00 to 1.00 V in 0.1 M LiTFSI DMF electrolyte solution with the analyte concentration of ca. 1−3 mg/mL. All potentials are reported vs the Fc/Fc^+ redox couple.

PETE Synthesis. All PETE samples were synthesized under stoichiometric vinyl ether−thiol ratios. **PETE-1** is presented here as a representative synthesis. To a 40 mL rubber sealed vial, 1.5 g of tri(ethylene glycol) divinyl ether (7.41 mmol), 1.35 g of 3,6-dioxa-1,8-octanedithiol (7.40 mmol), and 12.5 mL of dry THF were added. The solution was sparged with N_2 for 30 s, followed by the addition of 65 mg of Irgacure 2959 (0.298 mmol). The reaction was stirred and irradiated with UV light (365 nm) for 1 h using a 100 W Blak-Ray B-100 AP/R lamp. Solvent was removed by rotary evaporation, after which the sample was redissolved in a minimal volume of THF, and precipitated into diethyl ether (precipitation solvents for other samples were methanol for the **1**−**4** and diethyl ether for **5**−**8**). The sample was then dried under vacuum at 80 °C for 18 h (typical yield for **PETE** samples was 90%). ^{1}H NMR chemical shifts for PETE samples are presented below, while full spectra can be found in Figures S1−S8.

1: ^{1}H NMR (500 MHz, $CDCl_3$): δ 3.61 (4H, t, J = 6.7 Hz), δ 3.48 (4H, t, J = 5.2 Hz), δ 2.80 (4H, s), δ 2.75 (4H, t, J = 6.7 Hz), δ 1.66 (4H, b).

2: ^{1}H NMR (500 MHz, $CDCl_3$): δ 3.56 (4H, t, J = 6.8 Hz), δ 3.48 (4H, t, J = 6.1 Hz), δ 2.71 (4H, t, J = 6.7 Hz), δ 2.59 (4H, t, J = 6.7 Hz), δ 1.71 (4H, b), δ 1.66 (4H, b).

3: ^{1}H NMR (500 MHz, $CDCl_3$): δ 3.60 (4H, t, J = 7.1 Hz), δ 3.49 (4H, t, J = 6.1 Hz), δ 2.71 (4H, t, J = 7.0 Hz), δ 2.57 (4H, t, J = 7.0 Hz), δ 1.66 (4H, b), δ 1.61 (4H, b), δ 1.41 (4H, b).

4: ^{1}H NMR (500 MHz, $CDCl_3$): δ 3.60 (4H, t, J = 7.0 Hz), δ 3.48 (4H, t, J = 6.1 Hz), δ 2.71 (4H, t, J = 7.0), δ 2.56 (4H, t, J = 7.4 Hz), δ 1.66 (4H, bm), δ 1.60 (4H, b), δ 1.39 (4H, b), δ 1.31 (4H, b).

5: ^{1}H NMR (500 MHz, $CDCl_3$): δ 3.67 (12H, m), δ 2.77 (8H, m).

6: ^{1}H NMR (500 MHz, $CDCl_3$): δ 3.67 (12H, m) δ 2.78 (12H, m).

7: ^{1}H NMR (500 MHz, $CDCl_3$): δ 3.68 (12H, s), δ 3.66 (4H, t, J = 3.7 Hz), δ 2.79 (4H, s), δ 2.76 (4H, t, J = 6.7 Hz).

8: ^{1}H NMR (500 MHz, $CDCl_3$): δ 3.67 (16H, m), δ 2.78 (12H, m).

PETE-1. ^{1}H NMR (500 MHz, $CDCl_3$): δ 3.66 (24H, m), δ 2.77 (8H, t, J = 6.7 Hz).

Oxidation of PETE-1 to PESO-1. **PETE-1** was oxidized following previous reports of polyphosphazene oxidation.[24] To a 20 mL scintillation vial, 183 mg of **PETE-1** (1.32 mmol of thioether functional group) and 0.932 mL of 35% H_2O_2 in water (13.2 mmol) were added, followed by 9.3 mL of water. Though **PETE-1** was not initially soluble in water, the reaction was stirred overnight, after which no insoluble material remained. Residual H_2O_2 was removed by dialysis against RO water for 2 days. The polymer was then recovered by lyophilization (93% yield). **PES-1**: ^{1}H NMR (500 MHz, $CDCl_3$): δ 3.87 (8H, b), δ 3.60 (16H), b), δ 3.31 (8H, b).

Oxidation of PETE-1 to PES-1. In a 20 mL scintillation vial, 224 mg of **PETE-1** (1.62 mmol of thioether functional group) was dissolved in 4.5 mL of THF, followed by the addition of 1.4 g of *m*CPBA (8.11 mmol). After stirring overnight, the reaction had become opaque. Because the resulting polymer was insoluble in THF, the sample was chilled to −20 °C and the supernatant was decanted. The residual material was redissolved in a minimal volume of CH_2Cl_2 and precipitated into cold diethyl ether. The polymer was dried under vacuum for 18 h at 80 °C and recovered with a yield of 73%. **PES-1**: ^{1}H NMR (500 MHz, $CDCl_3$): δ 3.87 (8H, b), δ 3.60 (16H), b), δ 3.31 (8H, b).

Preparing Polymer Electrolytes. Polymer electrolytes were prepared by first dissolving a known amount of dried LiTFSI salt into an appropriate solvent (THF for **1**−**8** and **PETE-1**, 1:1 THF:MeOH for **PESO-1**, 1:1 CH_2Cl_2:MeOH for **PES-1**). The neat polymers were dissolved in the salt solution to obtain a r = [Li]/[FG] ratio of 0.05, 0.1, or 0.2, where [FG] is the total molar concentration of ether, thioether, sulfoxide, and sulfone functional groups. Polymer electrolyte samples were dried under vacuum at 80 °C overnight.

RESULTS AND DISCUSSION

Polymer Design. Two distinct series of PETEs were synthesized to establish structure−property relationships relating to polymer thermal properties and lithium ion mobility. Series A, polymers **1**−**4** (see Figure 1), was designed to examine the influence of carbon spacer length between thioether units, while the carbon spacer between ether functional groups was maintained at four methylene units. Series B, polymers **5**−**8**, maintained carbon spacer lengths between both heteroatoms at two methylene units but varied the thioether and ether ratio along the polymer backbone. Another sample, **PETE-1**, was made with the intention of comparing thioether, sulfoxide, and sulfone functional groups. This polymer was specifically designed to irregularly space out backbone sulfur atoms with ethylene oxide units, in the hopes of mitigating potential ionic cross-linking in electrolyte samples and to prevent the polymer from crystallizing.[24]

PETE Synthesis. THF GPC data for polymers **1**−**8** (Table 1) indicated polymers were successfully formed, with degrees of polymerization ranging from 55 to 90 after precipitation and drying (traces in Figure S9). Obtaining high molecular weight polymers by this method (>20 kg/mol) appears challenging, likely limited in part by intramolecular cyclization. Observed $Đ$ values varied from 1.6 to 2.1, with no particular dependence on degree of polymerization. Because of the step-growth nature of the thiol−ene condensation polymerization, dispersities of 2 were expected.[42] These numbers are likely lower due to low molecular weight species being fractionated out during precipitation, resulting in a narrowing of the dispersity on the low molecular weight end. This is demonstrated by comparing crude and precipitated GPC traces (Figure S10a). It is also

DOI: 10.1021/acs.macromol.5b02513
Macromolecules 2016, 49, 1154−1162

Table 1. Physical Properties of Polymers 1−8. Samples with * indicate multiple melting endotherms.

sample	M_n[a] (kg/mol)	$Đ$[a]	N[b]	T_g[c] (°C)	T_m[c] (°C)	ΔH[c] (J/g)
1	7.2	1.6	61	−61.8	*	*
2	8.8	2.0	67	−76.8	30.7	67.8
3	11.2	2.1	77	N/A	31.7	69.3
4	13.2	1.8	82	N/A	39.2	86.3
5	11.2	1.7	89	−58.7	*	*
6	11.7	1.7	75	N/A	70.0	61.1
7	10.1	1.7	69	−59.6	N/A	N/A
8	9.0	1.6	55	−50.1	56.8	83.0

[a]As determined by GPC using THF as the eluent against PS standards. [b]Calculated by averaged monomer weights. [c]As measured by DSC, heating at 10 °C/min.

apparent from this GPC trace that additional chain elongation occurs during drying, as all dried samples shift to lower retention times. This can be attributed to the increase in polymer end group concentration in the neat state, which can lead to further reaction. However, after drying a sample at higher temperatures a second time, no significant increase in molecular weight was observed, indicating long-term stability (Figure S10b). While disulfide linkages are possible, GPC data of **2** both with and without reducing agent DTT (Figure S10c) demonstrate no difference in molecular weight between the two, indicating that disulfide bonds are likely not contributing to this molecular weight increase. After precipitation, ^{1}H NMR confirmed pure polymer samples with peaks corresponding to protons adjacent to ethers and thioethers, with vinyl ether peaks remaining in some samples. Samples also displayed large ether stretches by FTIR, though no attempt to identify the thioether stretch was made due to its low intensity and location in the fingerprint region of the spectra.

Oxidation to PESO-1, PES-1. The selective oxidation of **PETE-1** to **PESO-1** was assessed by FTIR, NMR, and GPC. After stirring overnight in an aqueous H_2O_2 solution, a new stretch by FTIR appeared at 1030 cm^{-1}, corresponding to the sulfoxide stretching frequency (Figure 2a). ^{1}H NMR confirmed quantitative sulfoxide formation, where peaks corresponding to protons adjacent to thioethers (2.78 ppm) vanished, being replaced with a new downfield peak (3.27 ppm) corresponding to protons alpha to a sulfoxide (Figure 3). Overoxidation to the sulfone did not appear to occur under these conditions, as no characteristic sulfone peaks were present in FTIR (∼1300 cm^{-1}) or NMR (∼3.35 ppm). The oxidation of **PETE-1** to **PES-1** was characterized similarly. After purifying from the THF/*m*CPBA solution, the sulfone stretching frequency appeared by FTIR, observed as three peaks from 1250 to 1380 cm^{-1} (Figure 2a). ^{1}H NMR also showed a complete disappearance of thioether peaks and the presence of new peaks corresponding to protons adjacent to a sulfone (Figure 3). This two-step oxidation also appeared quantitative, as no indication of sulfoxide, either by FTIR or ^{1}H NMR, was present.

PETE-1, **PESO-1**, and **PES-1** were analyzed by DMF GPC because the oxidized products were insoluble in THF (Figure 2b). No peak shift or shape change was observed, indicating the polymer backbone integrity was maintained and that no major chain scission/fusion events occurred. It is worth noting that both **PESO-1** and **PES-1** are water-soluble polymers, whereas their precursor molecule **PETE-1** is not soluble.

FTIR of Polymers with Varying Salt Loadings. FTIR was also used to determine the coordination behavior of salt doped samples, at salt loadings of r = 0.05, 0.1, and 0.2. If salt is dissolving in the polymer and the ether oxygen is contributing to that solvation, a new stretch at a slightly lower wavenumber (∼1080 cm^{-1}) should be seen in addition to the standard ether stretch around 1100 cm^{-1}.[44,45] Samples **1**−**3** show a slight peak shift at loadings of r = 0.05 and 0.1 and a more prominent hump at lower wavenumber at r = 0.2. Sample **4**, however, has no observable peak change as salt loading is increased (Figure S11). Because of the more hydrophobic nature of the carbon spacer in **4**, it seems likely that the salt is not able to fully dissolve in this polymer at room temperature. In contrast, peak broadening at lower salt loadings and a clear new stretch around 1080 cm^{-1} at r = 0.2 were seen for **5** and **6**. Samples **7** and **8** also demonstrated broadening at 1100 cm^{-1}, though no new distinct peaks were observed (Figure S12). This data indicates improved salt solubility in samples with smaller carbon spacers.

PETE-1, **PESO-1**, and **PES-1** were also analyzed by FTIR at a variety of salt loadings (Figure S13). All three samples showed a similar trend with the respect to the ether stretch, as seen by a peak broadening at lower salt loadings and the development of the new peak at lower wavenumber at r = 0.2. A small shift in the sulfoxide stretching frequency was seen

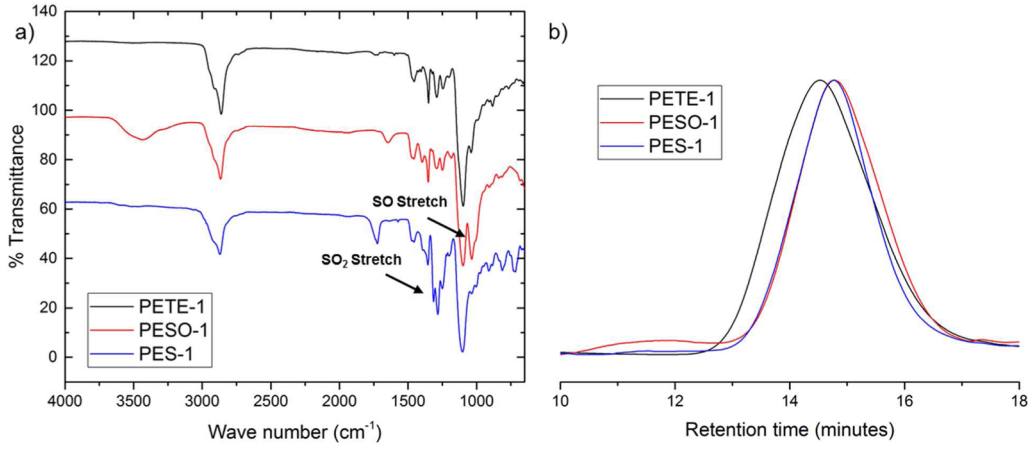

Figure 2. (a) Confirmation of the sulfoxide and sulfone functional groups by FTIR. (b) GPC traces of **PETE-1** and its oxidized products, **PESO-1** and **PES-1**. No major peak shift is detected.

DOI: 10.1021/acs.macromol.5b02513
Macromolecules 2016, 49, 1154−1162

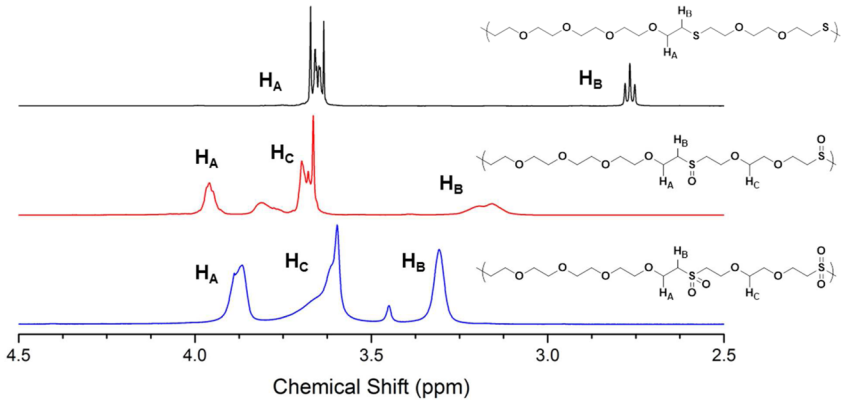

Figure 3. ^{1}H NMR ($CDCl_3$, 500 MHz) of **PETE-1** (top, black), **PESO-1** (middle, red), and **PES-1** (bottom, blue). The shift of H_B to higher ppm as well as a change in H_A and H_C demonstrates quantitative, selective oxidation to both polymers.

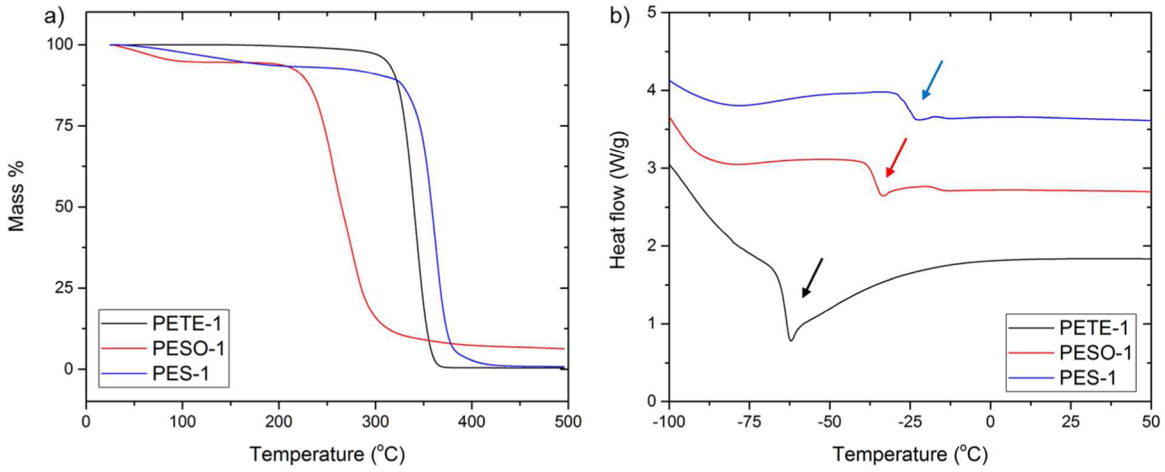

Figure 4. (a) TGA of **PETE-1** and its oxidized products, **PESO-1** and **PES-1** and (b) shifted DSC of the three neat samples, with T_g values indicated by arrows.

upon the addition of salt, though at higher salt loadings, the prominent LiTFSI peak obscures this shift. Regardless, it seems apparent that the sulfoxide functional groups are indeed interacting with the lithium salt due to the change in frequency even at lower salt loadings. In the case of **PES-1**, the three peaks corresponding to the sulfone have varying behavior. The center peak shows no shift as salt is added, but the stretches at slightly higher and lower wavenumbers both shift to slightly higher and lower values, respectively. At the highest salt loadings, both of these peaks begin to mix with signals from the LiTFSI salt. Based on these peak shifts, it appears that the sulfone group is also interacting with the lithium salt at all salt loadings.

Thermal Transitions and Stability. All samples were characterized for thermal stability by thermogravimetric analysis (Figure S14). Polymers **1**−**4** were thermally stable, generally up to about 250 °C, with 2% mass loss occurring between 237 and 264 °C. Samples **3** and **4** left incrementally more residual mass, possibly due to the larger carbon spacer length. Polymers **6**−**8** demonstrated similar thermal stability, with 2% mass loss occurring between 228 and 238 °C. Sample **5**, however, experienced 2% mass loss at 173 °C, with more gradual mass loss until around 300 °C, after which the sample rapidly decomposed. This is likely not due to residual monomer, as all samples were precipitated and thoroughly dried under vacuum. **PETE-1** followed a very similar decomposition route as polymers **1**−**8**, experiencing 2% mass loss at 286 °C (Figure 4a). **PESO-1** and **PES-1** both seem to be hygroscopic, as both show mass loss near the boiling point of water, representing between 4 and 6% of the total sample mass. After accounting for water mass, 2% mass loss for **PESO-1** and **PES-1** occurs at 215 and 294 °C, respectively. Regardless of water content, **PESO-1** seems significantly less thermally stable than its counterparts.

Samples were also analyzed by DSC to determine crystallinity and T_g (Tables 1 and 2). All DSC traces can be found in Figures S15−S20. As discussed earlier, a low T_g, corresponding to a higher rate of chain relaxations, leads to higher ion mobility and ultimately higher conductivity.[2,12] Samples **1** and **2** each displayed a prominent T_g when probed from −120 to 120 °C. Samples **1**−**4** all crystallized, with **1** experiencing two distinct melting points. As the carbon spacer length increased within samples **2**−**4**, the melting temperature

Table 2. T_g Values as a Function of Salt Loading

	T_g, with indicated salt loading (°C)			
sample	neat	r = 0.05	r = 0.1	r = 0.2
PETE-1	−63.6	−45.9	−52.5	−33.9
PESO-1	−35.5	−30.2	−19.2	−21.1
PES-1	−26.2	−7.1	−22.5	−20.8

DOI: 10.1021/acs.macromol.5b02513
Macromolecules 2016, 49, 1154−1162

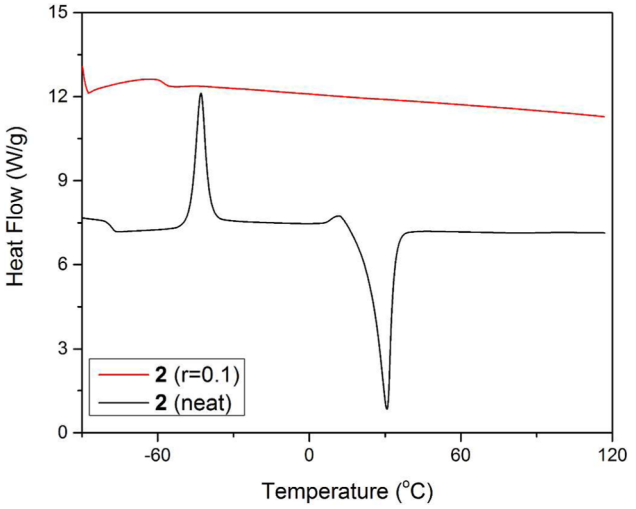

Figure 5. DSC of polymer **2** both with (top, red) and without (bottom, black) salt. Salt both increases T_g and suppresses crystallinity in this sample.

and endotherm increased, indicating more stable crystal formation. Polymer **2** also had a very large cold crystallization during heating at about 25 °C higher than its T_g. Doping these samples with a salt loading of r = 0.1 significantly changed thermal behavior. For **2**, all crystallization was suppressed and the T_g was slightly elevated, in a similar fashion to PEO (Figure 5). Samples **1**, **3**, and **4** retained crystallinity, though the magnitude of the melting endotherm was decreased, as was the melting temperature. Polymer **4**, the sample that did not demonstrate lithium ion coordination by FTIR, had the smallest change in endotherm magnitude and melting temperature, providing further evidence for a lack of lithium coordination.

Samples **5**, **7**, and **8** displayed prominent T_g values, between −50 and −60 °C, while **6** had no observed T_g. These values are similar to PEO, a feature arising possibly due to their similar backbone structure. Samples **5**, **6**, and **8** were all semicrystalline; **5** in particular demonstrated two distinct cold crystallizations and melting temperatures, a fact that was confirmed by heating the sample both at a rate of 1 and 10 °C/min (Figure S19). The addition of salt to these samples eliminated crystallinity and slightly elevated T_g in a manner again similar to PEO. These findings indicate that crystallinity in **5**, **6**, and **8** is driven by heteroatom interactions that can be disrupted by the addition of salt. Conversely, crystallinity in polymers **1**−**4** is more dependent on carbon chain alignment, which is unperturbed by salt. The lack of crystallization in **7** is likely due to the high ratio of backbone ethers to thioethers, arranged in such a way that prohibits packing.

DSC traces of **PETE-1**, **PESO-1**, and **PES-1** are shown in Figure 4b with tabulated T_g values shown in Table 2. As the oxidation state, and therefore polarity, of the sulfur-centered functional group increased, so did the T_g. This is unsurprising, as the increase in polarity allows for stronger dipole−dipole interactions, which would in turn increase the T_g. The low T_g values of **PESO-1** and **PES-1** are likely due to the irregular spacing along the backbone, alternating between two and four ethylene oxide unit spacers. No crystallinity was observed for these three samples. The addition of salt to these polymers increased T_g, generally increasing in magnitude with higher salt loadings. While it is difficult to decouple the contributions of low T_g values and more polar functional groups to conductivity, **PES-1** and **PESO-1** have very similar T_g values at the salt loading r = 0.2, and a direct comparison of conductivity values will thus be made in the next section. Though observing nonlinear increases in T_g versus salt loading for PEO based SPEs is not entirely uncommon,[46] we believe there may be two separate coordination events at different salt concentrations occurring (Li−SO/SO_2, and Li−O) that cause this particular nonlinear relationship. Overall, the low T_g values of these tailored materials and their lack of crystallinity, either neat or with salt, are encouraging properties of SPE candidates.

Lithium Ion Mobility. To assess lithium ion conductivity, polymers were characterized by EIS. The effect on conductivity of carbon spacer length between thioether units, of the ratio and sequence of thioether and ether units, and of the oxidation state of sulfur in the backbone was evaluated. As sulfur atoms are significantly larger than oxygen atoms, a larger carbon spacer may promote coordination and mobility, even though the spacer adds hydrophobicity.[21] Lithium conductivity of **1**−**4** at a salt loading of r = 0.1 is shown in Figure 6a and at salt loadings of r = 0.05 and 0.2 in Figure S21. All polymers within this series conducted similarly, with **2** and **3** demonstrating nearly identical temperature dependence. While these samples had the highest conductivity values of the series, **1** was nearly as high, indicating that adding up to six methylene spacers had

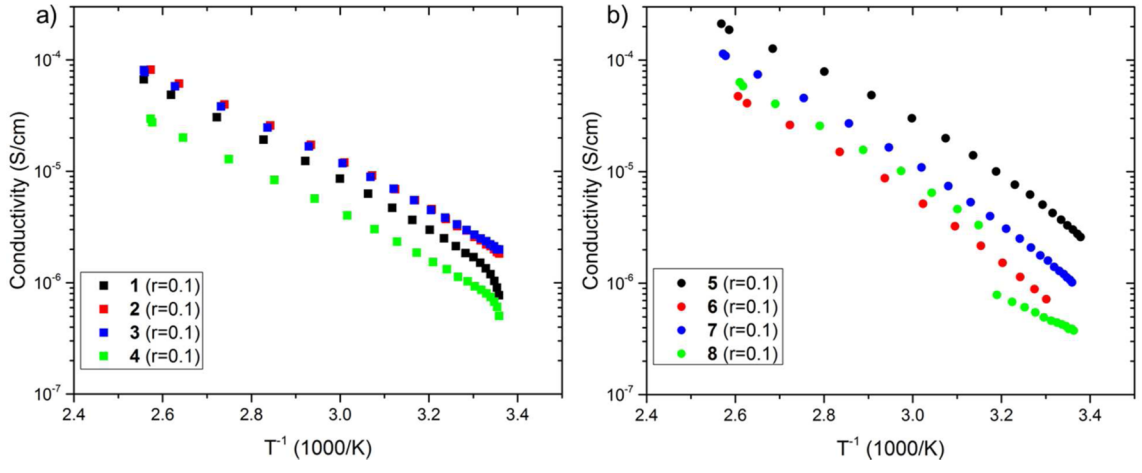

Figure 6. Temperature-dependent conductivity by EIS of (a) samples **1**−**4** (squares) and (b) samples **5**−**8** (circles).

DOI: 10.1021/acs.macromol.5b02513
Macromolecules 2016, 49, 1154−1162

very little impact on lithium ion mobility. In contrast, **4** had the lowest conductivity of the series, demonstrating that increasing the carbon spacer length does eventually hinder conductivity. Low conductivity for **4** is not entirely surprising, as both FTIR and DSC data revealed weak ether−lithium interactions and an inability to disrupt crystallinity, respectively. Thus, the long spacer length may be detrimental due to a lower concentration of coordinating atoms and the increase in crystallization. Interestingly, both **1** and **4** show a dropoff in conductivity at low temperatures, consistent with crystallinity. Both of these materials retain some crystallinity with salt, as shown in Figure S15.

Polymers **5**−**8** demonstrated similar conductivities when compared to **1**−**4**. Samples in this low carbon spacer length series also generally conducted very similarly, with polymers containing only two thioethers per repeat unit performing the best. This does not necessarily indicate that ethers are more critical than thioethers for high conductivity, as **5**, with a higher S to O ratio, outperformed **7**. A sharp decrease in conductivity for sample **8**, demonstrative of crystallization, was also observed. This crystallization is not apparent in the final heating cycle of DSC but can be seen during the first heating cycle (Figure S20). The slight improvement in conductivity in the series **5**−**8** over **1**−**4** is likely due to the four-carbon spacer present between ether units in **1**−**4**. Alkylene oxide materials show a strong conductivity dependence on carbon spacer between ethers, where polymers with two methylene units (PEO) performing better than materials deviating from that.[47,48] While there is no polymer in this report that is a direct comparison between the two polymer series, based on the similar conductivity curves for **1**−**4**, it appears that carbon spacer length between ethers is more relevant to conductivity than spacer lengths between thioethers. It also seems that for samples **1**−**8** there is a dependence of conductivity on salt loading, specifically higher salt loadings yield improved conductivities. This is not entirely consistent with PEO based SPEs, where the optimal salt loading has been found to be r = 0.085, and might suggest subtle differences in conductivity mechanisms.[49] However, these findings are supported by the thermal characterization at all salt loadings for samples **2** and **7** (Figure S17). The lowest T_g observed for these samples with salt was at the highest salt loading (r = 0.2), which should lead to the highest conductivity.

PETE-1, **PESO-1**, and **PES-1** were also characterized by EIS to determine lithium conductivity as the oxidation and polarity of the sulfur atoms along the polymer backbone increased. As mentioned earlier, these three polymers have irregular repeat units, with the sulfur functional groups separated by two and four ethylene oxide units to inhibit crystallization and decrease T_g in the hopes of improving ion mobility. The increase in polarity should strengthen the polymer−lithium interaction, mimicking the stronger interactions associated with solvents found in liquid battery electrolytes.[50] Temperature-dependent conductivity at a salt loading of r = 0.1 for these three polymers is shown in Figure 7 and at salt loadings of r = 0.05 and 0.2 in Figure S22. **PETE-1** conducts similarly to sample **5**, if not better, and begins to approach PEO levels of conductivity at a salt loading of r = 0.05.[49] This may indicate that decreasing the relative number of thioethers to ethers, thus making the polymer more like PEO, improves conductivity. Furthermore, **PETE-1** is completely amorphous at r = 0.05, unlike PEO, indicating that **PETE-1** has a very broad temperature window for effective conductivities. Additionally, this finding suggests

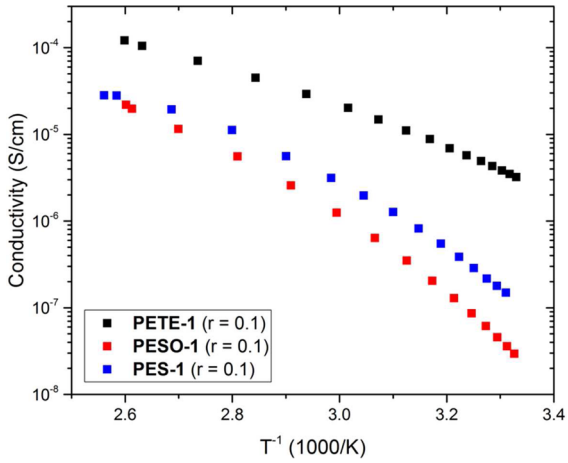

Figure 7. Lithium ion conductivity by EIS at a salt loading of r = 0.1 for **PETE-1**, **PESO-1**, and **PES-1**.

that the sequence of the thioethers and ethers is inconsequential. The two-step oxidation to **PES-1** yields a polymer with lower conductivity by roughly an order of magnitude. Interestingly, the single oxidation to **PESO-1**, with a lower dipole moment than **PES-1**, yields the lowest conductivity of the series. It should be noted that though **PESO-1** has high water content by TGA, the samples were thoroughly dried for 4 h under vacuum at 120 °C, and water is not expected to be present during EIS measurements. The more highly oxidized samples (**PESO-1**, **PES-1**) demonstrate higher conductivities at higher salt loadings. This may be due to a salt titration effect, wherein at low salt loadings, lithium is strongly bound to highly polar groups, but at higher loadings where there are no free polar groups, lithium becomes more mobile. These three samples were also assessed for electrochemical stability by linear scanning voltammetry (Figure S23). Generally, samples were stable, though **PETE-1** demonstrated a small transition at −0.4 V.

There are two competing factors that dictate ion mobility for polymers **PETE-1**, **PESO-1**, and **PES-1**: chain mobility and polymer polarity.[2] At a salt loading of r = 0.1, conductivity seems to trace roughly with inverted T_g, where samples with lower T_g values demonstrate higher conductivities. This is well understood for poly(alkylene oxide)s, where an increase in T_g corresponds to a decrease in chain relaxations and ion mobility. Here, chain mobility is likely a factor and is unfortunately intimately connected to the parameter being probed: polymer polarity. At a salt loading of r = 0.2, **PESO-1** and **PES-1** have nearly identical T_g values, but **PES-1** conducts roughly 3 times as well (Figure S22). Because of the similarity in T_g, backbone polarity is isolated as a variable, which demonstrates here that sulfones are more advantageous for lithium ion mobility. By further optimization through this platform, it may be possible to obtain sulfone containing or highly polar materials with even lower T_g values and higher lithium ion conductivity.

CONCLUSIONS

Poly(ether−thioethers) were synthesized using a step-growth thiol−ene click-mediated polymerization. Two series of PETEs, one varying methylene units between thioethers and one varying the ratio of ethers to thioethers, were synthesized and characterized neat and as lithium−polymer electrolytes. Polymers with methylene spacers of two, four, and six all

DOI: 10.1021/acs.macromol.5b02513
Macromolecules 2016, 49, 1154−1162

conducted similarly, while the sample with eight methylene units had lower ion mobility. All samples in this series were crystalline and showed decreased crystallinity upon the addition of salt. Varying the ratio of ethers to thioethers had a more subtle effect, though samples in this series, all with short two methylene carbon spacers between heteroatoms, conducted lithium slightly better than the previous series.

Another polymer, **PETE-1**, was synthesized to have long, irregular spacings between thioether units. This sample was selectively oxidized to a sulfoxide, **PESO-1**, and a sulfone, **PES-1**. The increase in polarity of these polymers also resulted in an increase in T_g, with **PETE-1** at −64 °C, **PESO-1** at −36 °C, and **PES-1** at −26 °C. **PETE-1** demonstrated higher lithium ion mobility at all salt loadings probed (r = 0.05, 0.1, 0.2) and was comparable to PEO, likely due to its low T_g. At a salt loading of 0.2, however, **PESO-1** and **PES-1** demonstrated similar T_g values, while **PES-1** maintained a higher conductivity than **PESO-1**. This finding demonstrates both the importance of highly polar functional groups capable of coordinating and shuttling lithium ions and backbone mobility. The polymers synthesized in this work represent a new class of materials for structure−property studies of solid polymer electrolytes. In addition, this synthetic approach opens avenues to novel mixed heteroatom polymers, including redox tunable thioether groups. For example, **PESO-1** and **PES-1** are water-soluble, but their precursor, **PETE-1**, is not. Varying the monomers used to make these, and other, polymers will yield new tunable redox-sensitive materials, with a wide variety of potential applications.

■ ASSOCIATED CONTENT

Supporting Information

The Supporting Information is available free of charge on the ACS Publications website at DOI: 10.1021/acs.macromol.5b02513.

^{1}H NMR, GPC, TGA, DSC, FTIR, and EIS data (PDF)

■ AUTHOR INFORMATION

Corresponding Author

*E-mail tew@mail.pse.umass.edu (G.N.T.).

Notes

The authors declare no competing financial interest.

■ ACKNOWLEDGMENTS

This work was funded by the Office of Naval Research Grant N00014-10-1-0348. The authors thank Ms. Coralie Backlund and Ms. Kelly McLeod for their assistance in preparing the manuscript. The authors also acknowledge Prof. Tom McCarthy, Prof. Mark Touminen, Mr. Daniel Flagg, and Mr. Ramesh Adhikari for maintaining and allowing access to private instrumentation. Special thanks goes to Mr. Ryan Selhorst for his assistance with linear scanning voltammetry.

■ REFERENCES

(1) Tarascon, J. M.; Armand, M. *Nature* **2001**, *414*, 359−367.
(2) Hallinan, D. T.; Balsara, N. P. *Annu. Rev. Mater. Res.* **2013**, *43*, 503−525.
(3) Chintapalli, M.; Chen, X. C.; Thelen, J. L.; Teran, A. A.; Wang, X.; Garetz, B. A.; Balsara, N. P. *Macromolecules* **2014**, *47*, 5424−5431.
(4) Panday, A.; Mullin, S.; Gomez, E. D.; Wanakule, N.; Chen, V. L.; Hexemer, A.; Pople, J.; Balsara, N. P. *Macromolecules* **2009**, *42*, 4632−4637.
(5) Wang, X.; Thelen, J. L.; Teran, A. A.; Chintapalli, M.; Nakamura, I.; Wang, Z.-G.; Newstein, M. C.; Balsara, N. P.; Garetz, B. A. *Macromolecules* **2014**, *47*, 5784−5792.
(6) Teran, A. A.; Mullin, S. A.; Hallinan, D. T.; Balsara, N. P. *ACS Macro Lett.* **2012**, *1*, 305−309.
(7) Hawker, C. J.; Chu, F.; Pomery, P. J.; Hill, D. J. T. *Macromolecules* **1996**, *29*, 3831−3838.
(8) Barteau, K. P.; Wolffs, M.; Lynd, N. A.; Fredrickson, G. H.; Kramer, E. J.; Hawker, C. J. *Macromolecules* **2013**, *46*, 8988−8994.
(9) Allcock, H. R.; Bender, J. D.; Morford, R. V.; Berda, E. B. *Macromolecules* **2003**, *36*, 3563−3569.
(10) Zhang, Z. C.; Jin, J. J.; Bautista, F.; Lyons, L. J.; Shariatzadeh, N.; Sherlock, D.; Amine, K.; West, R. *Solid State Ionics* **2004**, *170*, 233−238.
(11) Allcock, H. R.; Austin, P. E.; Neenan, T. X.; Sisko, J. T.; Blonsky, P. M.; Shriver, D. F. *Macromolecules* **1986**, *19*, 1508−1512.
(12) Kuan, W.-F.; Remy, R.; Mackay, M. E.; Epps, T. H., III *RSC Adv.* **2015**, *5*, 12597−12604.
(13) Tominaga, Y.; Shimomura, T.; Nakamura, M. *Polymer* **2010**, *51*, 4295−4298.
(14) Tominaga, Y.; Yamazaki, K.; Nanthana, V. *J. Electrochem. Soc.* **2015**, *162*, A3133−A3136.
(15) Tominaga, Y.; Nanthana, V.; Tohyama, D. *Polym. J.* **2012**, *44*, 1155−1158.
(16) Webb, M. A.; Jung, Y.; Pesko, D. M.; Savoie, B. M.; Yamamoto, U.; Coates, G. W.; Balsara, N. P.; Wang, Z.-G.; Miller, T. F. *ACS Cent. Sci.* **2015**, *1*, 198−205.
(17) Watanabe, Y.; Kinoshita, S. I.; Wada, S.; Hoshino, K.; Morimoto, H.; Tobishima, S. I. *J. Power Sources* **2008**, *179*, 770−779.
(18) Watanabe, M.; Nagano, S.; Sanui, K.; Ogata, N. *Polym. J.* **1986**, *18*, 809−817.
(19) Wong, D. H. C.; Thelen, J. L.; Fu, Y.; Devaux, D.; Pandya, A. A.; Battaglia, V. S.; Balsara, N. P.; DeSimone, J. M. *Proc. Natl. Acad. Sci. U. S. A.* **2014**, *111*, 3327−3331.
(20) Clancy, S.; Shriver, D. F. *Macromolecules* **1986**, *19*, 606−611.
(21) Johansson, P. *Polymer* **2001**, *42*, 4367−4373.
(22) Cheng, Q.; Cui, Z.; Li, J.; Qin, S.; Yan, F.; Li, J. *J. Power Sources* **2014**, *266*, 401−413.
(23) Wu, F.; Zhou, H.; Bai, Y.; Wang, H.; Wu, C. *ACS Appl. Mater. Interfaces* **2015**, *7*, 15098−15107.
(24) Allcock, H. R.; Olmeijer, D. L. *Macromolecules* **1998**, *31*, 8036−8046.
(25) Hoyle, C. E.; Bowman, C. N. *Angew. Chem., Int. Ed.* **2010**, *49*, 1540−1573.
(26) Hoyle, C. E.; Lee, T. Y.; Roper, T. *J. Polym. Sci., Part A: Polym. Chem.* **2004**, *42*, 5301−5338.
(27) Hoyle, C. E.; Lowe, A. B.; Bowman, C. N. *Chem. Soc. Rev.* **2010**, *39*, 1355−1387.
(28) Gress, A.; Völkel, A.; Schlaad, H. *Macromolecules* **2007**, *40*, 7928−7933.
(29) Barbey, R.; Perrier, S. *Macromolecules* **2014**, *47*, 6697−6705.
(30) van Hensbergen, J. A.; Gaines, T. W.; Wagener, K. B.; Burford, R. P.; Lowe, A. B. *Polym. Chem.* **2014**, *5*, 6225−6235.
(31) Lowe, A. B.; Liu, M.; van Hensbergen, J. A.; Burford, R. P. *Macromol. Rapid Commun.* **2014**, *35*, 391−404.
(32) Walker, C. N.; Sarapas, J. M.; Kung, V.; Hall, A. L.; Tew, G. N. *ACS Macro Lett.* **2014**, *3*, 453−457.
(33) Walker, C. N.; Versek, C.; Touminen, M.; Tew, G. N. *ACS Macro Lett.* **2012**, *1*, 737−741.
(34) Marvel, C. S.; Chambers, R. R. *J. Am. Chem. Soc.* **1948**, *70*, 993.
(35) Marvel, C. S.; Cripps, H. N. *J. Polym. Sci.* **1952**, *8*, 313.
(36) Marvel, C. S.; Markhart, H. *J. Polym. Sci.* **1951**, *6*, 711.
(37) Marvel, C. S.; Kotch, A. *J. Am. Chem. Soc.* **1951**, *73*, 481.
(38) Marvel, C. S.; Hinman, C. W.; Inskip, H. K. *J. Am. Chem. Soc.* **1953**, *75*, 1997.
(39) Park, M. J.; Balsara, N. P. *Macromolecules* **2010**, *43*, 292−298.
(40) Marvel, C. S.; Aldrich, P. H. *J. Am. Chem. Soc.* **1950**, *72*, 1978.
(41) Marvel, C. S.; Nowlin, G. *J. Am. Chem. Soc.* **1950**, *72*, 5026.

DOI: 10.1021/acs.macromol.5b02513
Macromolecules 2016, 49, 1154−1162

(42) Deubel, F.; Bretzler, V.; Holzner, R.; Helbich, T.; Nuyken, O.; Rieger, B.; Jordan, R. *Macromol. Rapid Commun.* **2013**, *34*, 1020−1025.
(43) Meyer, W. H. *Adv. Mater.* **1998**, *10*, 439−448.
(44) Wen, S. J.; Richardson, T. J.; Ghantous, D. I.; Striebel, K. A.; Ross, P. N.; Cairns, E. J. *J. Electroanal. Chem.* **1996**, *408*, 113−118.
(45) Huang, J.; Wang, R.; Tong, Z.; Xu, J.; Fan, Z. *Macromolecules* **2014**, *47*, 8359−8367.
(46) Stolwijk, N. A.; Heddier, C.; Reschke, M.; Wiencierz, M.; Bokeloh, J.; Wilde, G. *Macromolecules* **2013**, *46*, 8580−8588.
(47) Dias, F. B.; Plomp, L.; Veldhuis, J. B. J. *J. Power Sources* **2000**, *88*, 169−191.
(48) Akbulut, O.; Taniguchi, I.; Kumar, S.; Shao-Horn, Y.; Mayes, A. M. *Electrochim. Acta* **2007**, *52*, 1983−1989.
(49) Teran, A. A.; Tang, M. H.; Mullin, S. A.; Balsara, N. P. *Solid State Ionics* **2011**, *203*, 18−21.
(50) Arora, P.; Zhang, Z. *Chem. Rev.* **2004**, *104*, 4419−4462.

DOI: 10.1021/acs.macromol.5b02513
Macromolecules 2016, 49, 1154−1162